Hindawi
Journal of Nanomaterials
Volume 2022, Article ID 8503507, 11 pages
https://doi.org/10.1155/2022/8503507

Research Article

Mathematical Model and Simulation Calculation Method Based on the Exfoliation of Single-Layer Graphene from Dispersed Carbon Nanotubes

Xudong Sha and Li Zhao

Department of Mathematics and Physics, Zibo Normal College, Zibo, 255100 Shandong, China

Correspondence should be addressed to Li Zhao; 9029001017@zbnc.edu.cn

Received 5 March 2022; Revised 11 May 2022; Accepted 23 May 2022; Published 14 June 2022

Academic Editor: Awais Ahmed

Graphene is a two-dimensional material with excellent performance and unique structure. Since its successful manufacturing in 2004, it has quickly become a research hotspot in the fields of materials, chemistry, physics, and engineering. This article focuses on the study of exfoliated single-layer graphene based on dispersed carbon nanotubes and understands the related theories of carbon nanotubes and exfoliated single-layer graphene on the basis of literature data. The mathematical model and simulation calculation method are analyzed, and then, the effect of the single-layer graphene peeling based on the dispersed carbon nanotubes is tested, mainly to the experimental verification of the peeling process parameters and the influence of the dispersant on the peeling effect, and then, the peeled graphite quality of the graphene was tested, and the test results showed that the thickness of single-layer pure graphene is 0.6-0.9 nm, and the experimental statistics show that the graphene of single-layer and double-layer occupies 81% of the experimental sample; most of the single-layer graphene exfoliated based on dispersed carbon nanotubes in this paper is single-layer, two-layer graphene, and a relatively small amount of multilayer graphene.

1. Introduction

In recent years, due to the widespread application of computer technology and the mature development of computing technology, a new round of scientific and technological revolution has been produced for computer simulation methods [1, 2]. In addition to theoretical research and empirical analysis, computer molecular simulation has also become another important scientific investigation method for people to understand the microcosm. At the same time, it is the main tool and method for new material design research [3, 4]. The computer extracts numerical values related to atomic diffusion coefficient, electron diffusion orbital through dynamic simulation, and numerical values that cannot be reflected in theoretical research or experiments [5, 6].

As a major type of petrochemical raw material, carbon nanotubes are widely used in the separation, refining, and processing of products in the chemical industry such as petrochemical, gasoline, and natural gas [7]. The special physical properties of various aspects, such as electricity, have attracted the attention of foreign scientists [8, 9].

The natural absorption isotherms of hydrogen atoms in pore size carbon nanotubes at different working temperatures have been found that under high and low temperature conditions, a moderate increase in the diameter of the carbon tube can also help hydrogen storage [10]. Therefore, some researchers have developed almost equivalent models to analyze the mechanical properties of carbon tubes used as reinforcement materials. The research results show that when the total integral number of carbon nanotubes is fixed, the measured value of sidewall/resin carbon nanotubes

increases as the diameter of carbon nanotubes increases and continues to remain constant after exceeding the specified value. When the diameter of carbon nanotubes reaches sixty to eighty nanometers, the strength of the single-wall carbon/composite is maximized. When the volume fraction of carbon nanotubes changes, it can be found that as the volume fraction of carbon nanotubes increases, the measured value of Young's axis also increases accordingly. In other words, when the volume fraction of carbon tubes reaches 25%, the axial elastic modulus of the composite resin with the same orientation of carbon nanotubes can reach 330 GPa. At the same time, in the case of composite resins in which carbon nanotubes are randomly distributed in the range of 0 to 7%, as the volume fraction of carbon nanotubes increases, the measured value also increases [11]. Some researchers studied the exfoliated graphene and chose N,N-dimethylpropylamine, N-(3-dimethylaminopropyl)methacrylamide, and 2-(tert-butylamino)methylacetonitrile. As a solvent, it participates in the production of graphene, but because the content of the graphene diffuser produced by it varies greatly and, at the same time, due to the continuous expansion of raw materials and the continuous peeling of the precipitate, the content of graphene in the solution reaches 15 mg/mL^{-1}. This is due to the strong interaction between the substance in the solution and the graphene. Therefore, the interaction between the solvent and graphene is the key reason for determining the content of graphene in the solution, and it is also the main reason to consider when choosing the solvent [12]. Some researchers used three different molecular ratios. The preparation of graphene solution was studied through the three-proportion system method. The above three parts of the mixed solution must be mixed at a high speed of 120 revolutions per minute for ten minutes before use, and the solution and the coloring solvent must be thoroughly mixed. When the molar ratio of BA reached 1 : 3, the dispersed content of graphene was as high as 6.5 mg/mL. When the NBA molar ratio reaches 1 : 4, the graphene content is only 0.09 mg/mL, and when the molar ratio reaches 1 : 3, it is only one-72nd, and it also shows that this ratio will make the n-butanol molecule internal self-bonding generated, so that the individual DMF solution can be stripped to obtain graphene, but different mixed solutions can neither guarantee the dispersion stability of graphene nor the stability of the graphene diffusion liquid, so different mixed solutions can affect graphene. The diffusion concentration produced a great difference [13]. This type of research lacks data support, and the conclusions drawn are still open to question. In summary, the research on the preparation of graphene has attracted much attention, but the preparation process is affected by many factors, so it is necessary to investigate these factors in depth.

This paper studies the exfoliation of single-layer graphene based on dispersed carbon nanotubes and analyzes the structure of carbon nanotubes, the preparation method of exfoliated single-layer graphene, and the factors affecting the stripping effect on the basis of literature data. Research is carried out based on the mathematical model and simulation calculation method of the single-layer graphene exfoliated by dispersed carbon nanotubes, and then, the graphene exfoliated by this method is tested, and relevant conclusions are drawn from the test results.

2. Carbon Nanotubes and Exfoliated Single-Layer Graphene

2.1. The Structure of Carbon Nanotubes. The basic structure of the carbon tube can be obtained using graphene sheet mapping [14]. The grid of the graphite sheet is represented by the vector $C = na_1 + ma2$ (n and m are integers, and a_1 and a_2 are the unit vectors of the graphite layer) [15]. The basic process of using flat grid points in the graphite layer to make carbon nanotubes is shown in the figure: starting from grid point zero, first use grid point A to establish grid vector C, and then, establish a line perpendicular to vector C, and then use points O and B to indicate. This point is a threaded grid point in the two-dimensional layer of the graphite layer, and the vector OB is a convertible vector, represented by T (see Figure 1). The straight line OD is a line parallel to the unit vector A, and the angle between the carbon-carbon bond of the hexagonal lattice perpendicular to the vector ODC and the sawtooth axis along the sawtooth axis of the hexagonal graphite lattice and the OD is θ. A line C passing through the spiral vector perpendicular to point A and a line perpendicular to point OB intersect at point B at point B'. The atomic weight contained in the rectangular OAB′B is the atomic weight contained in the single-walled carbon nanotube unit cell. On the axis OB, roll the powder sheet and align OB and A with the axis AB′ or align the axis OB with the axis AB′ to form the circumference of the main body of single-walled carbon nanotubes, and form the single-walled carbon tube of the main body at OB; the OA is formed around the single-walled carbon tube. Throughout the development process, it has been found that two parameters (n and m) can be used to describe single-walled carbon tubes. Regardless of the attribute, the structure of single-walled carbon nanotubes is completely determined by two quantities (n and m) (diameter and helix angle or both showing the graphite sheet structure index or helix vector C and translation vector T). Therefore, only selecting the spiral vector C of the graphite mesh determines the basic structure of the carbon tube and various technical parameters [16].

2.2. Preparation Method of Exfoliated Single-Layer Graphene

2.2.1. Mechanical Peeling Method. The mechanical peeling method, as the name implies, is to use external physical and mechanical forces to resist the van der Waals force between the toner layers to peel the toner [17]. The raw material often used here is highly oriented pyrolytic graphite. The process of manufacturing graphene involves gradually grinding centimeter-sized graphite blocks into smaller graphite flakes, and then grinding them into nanoscale graphite flakes. Graphite flakes continue to decompose and become thinner and thinner.

2.2.2. Liquid Phase Exfoliation Method. The liquid phase exfoliation method is a solution that can be produced

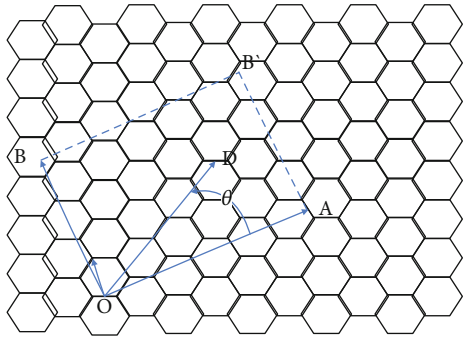

Figure 1: Schematic diagram of graphene sheet mapping to carbon nanotubes.

industrially, and it is also suitable for the manufacture of graphene composite materials [18]. The exfoliation method must overcome the van der Waals force between graphite layers, and the diffusion of graphite in liquid is the most direct and effective way to reduce the van der Waals force. Therefore, the liquid phase exfoliation method generally includes the following three stages: (1) the diffusion process of graphite in the solvent; (2) the auxiliary exfoliation by means of ultrasound, microwave, shear, heating, and electrochemistry; and (3) graphite obtained by centrifugation. The exfoliation preparation of graphene solution can include two types of substances: direct liquid phase exfoliation and auxiliary liquid phase exfoliation [19]. Figure 2 is a schematic diagram of the principle that the solvent disperses graphene in the solution smoothly.

2.2.3. Chemical Vapor Deposition Method. After decomposing some carbon-containing compounds, other forms of carbon can be converted to graphitic carbon. In subsequent catalysis experiments, the researchers found that the contact of hydrocarbons or carbon vapor with nickel or single crystal platinum can also form a graphite layer [20]. Subsequent studies have shown that the filled *d* orbitals of transition metals can absorb some carbon atoms. This provides a basis for the preparation of graphene by CVD [21]. When the carbon material is decomposed at a high temperature, the carbon atoms combine with the metal to form a carbon source. Due to the limited amount of molten metal carbon, sp2 hybrid carbon is deposited to form graphene. The type, concentration, and duration of the carbon source introduced during the deposition process have a significant impact on the size and number of graphene layers obtained. Figure 3 shows the preparation process of the CVD method.

2.2.4. Granulator Method. When the granulator rotates at a high speed, the water tank on the granulator rotates around the main shaft of the turntable and rotates around its own main shaft, thereby realizing planetary motion. Under the influence of high-speed centrifugal force, the crushing ball and the material in the tank rotate together at high speed, and a higher kinetic energy is formed in the relative movement between the crushing ball and the material. The shear stress and compressive stress between them cause the material to be stripped and crushed. The use of granulation in graphene production roughly includes wet granulation and dry granulation. The main medium of granulation is organic solvent (such as DMF, NMP, and cyclobutane) [22].

2.3. Factors Affecting Peeling Effect. Because the surface energy of graphene is high, the surface energy of the solution selected in the production process must be consistent with the surface energy of graphene, and it can diffuse into the solution stably. But at the same time, solutions suitable for exfoliating graphene are usually expensive and toxic. Water is the most commonly used solution, which is relatively safe and has the highest biocompatibility. However, the surface tension of water is far from that of graphene. Regarding this issue, R&D personnel have done a lot of research and added surfactants to adjust the H tendency so that the graphene is exfoliated from the water phase [23].

2.4. Simulation Calculation Method. Molecular simulation is usually a classic engineering-based research method, including molecular engineering, Monte Carlo, and molecular dynamic simulation [24]. This method regards the molecular model or system as a classical engineering model and calculates the molecular energy by repeatedly sampling the constitutive space of the molecular system to obtain the molecular orbital and structural properties. Molecular dynamic (MD) simulation is a type of molecular simulation that not only studies the structural properties of molecular systems but also analyzes the thermodynamics, migration, and chemical properties of the system. Therefore, it is widely used in materials, biopharmaceuticals, chemistry, and other fields.

(1) The molecular dynamic simulation process is mainly composed of the following three parts. (1) Calculate the total kinetic energy of the entire system. (2) Calculate the internal force of each molecule (atom) from the relationship between kinetic energy and force. Then, according to Newton's classical mechanics, the position of the atom can be inferred. (3) Solve physical quantities such as dynamics and thermodynamic properties according to the structural properties of the system [25]

(2) Some important issues in molecular dynamic simulation

2.4.1. Potential manipulation and energy optimization. Dynamic function is a form of function that controls the interaction force between atoms, which directly determines the dynamic energy of a system composed of different atoms, and is the most important parameter to control dynamic simulation [26]. For each atom, various potential characteristics must be selected to explain the interaction between them. A typical potential function is usually formed by superimposing various forms of interaction between individuals, such as the following equation:

$$U = \sum U_{bonds} + \sum U_{angles} + \sum U_{dihedral} + \sum U_{improper} + \sum U_{inverison} + \sum U_{cross} + \sum U_{\text{int } er}. \quad (1)$$

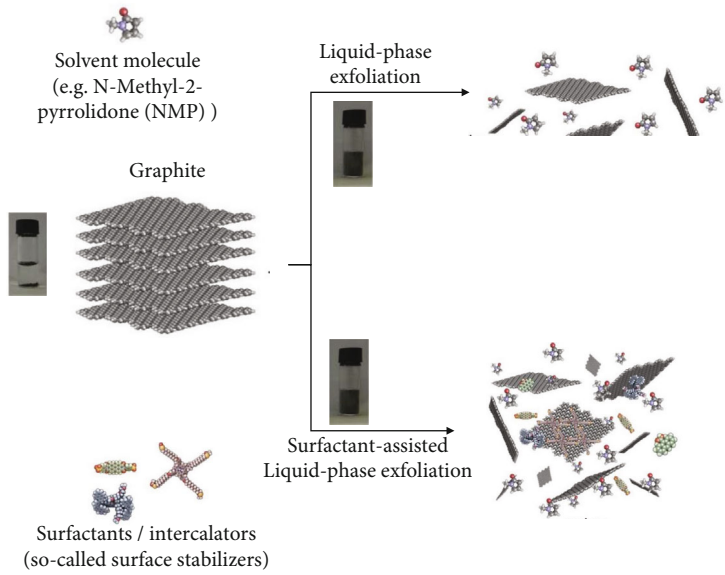

Figure 2: Liquid phase exfoliation (LPE) process.

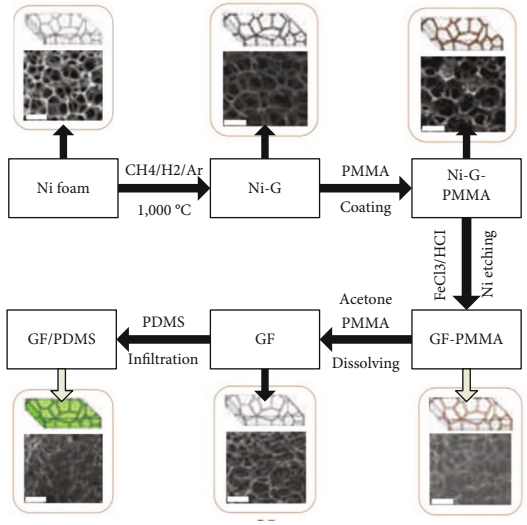

Figure 3: Schematic illustration of the preparation of grapheme by CVD method.

In the formula, the following are shown: (1) the potential energy caused by the expansion and contraction of the bond; (2) potential energy caused by the bending of the bond angle; (3) the potential energy when the dihedral angle deviates from the equilibrium position; (4) potential energy caused by pseudo-distortion; (5) potential energy caused by face flip; (6) interaction, potential energy caused by coupling; and (7) intramolecular nonbond interaction.

2.4.2. Conditions. In order to generate relatively accurate regular statistical data and accurately predict the macroscopic properties of materials and structures, it is necessary to perform MD simulations on systems with a large number of microscopic particles. However, due to the limitations of existing calculation conditions, up to 108 particles can be simulated, which is different from the macroscopic size, which is not enough at present. Periodic restrictions are usually introduced in the dynamic simulation to eliminate the restrictions as much as possible. In other words, the creation of a central unit gives a period limit that allows the system to recur in space and expands the system to infinity [27].

2.4.3. Overall and temperature and pressure control. MD simulates the motion of the system on the atomic scale, and the molecules perform a large amount of thermal motion. Therefore, statistics must be performed on the system containing a large number of particles to represent the statistical sample. In addition, the system for studying thermodynamics cannot be infinite, it must be finite. In quantum mechanics, the sum of the quantum states of each small particle in a thermodynamic system is its microscopic state. As a statistical engineering concept, the collection represents a collection of thermodynamic systems with the same macroscopic state but not necessarily the same microscopic state. The macroscopic state of the thermodynamic system mainly includes temperature (T), pressure (P), volume (V), and energy (E). Therefore, in the case of the same chemical composition of the system, the set can be divided into volume and energy harvesting NVE ensemble, pressure and temperature NPT set, same volume and temperature NVT set, etc.

When different holistic therapies are used in the system, the molecules in the system are in different states. Therefore, for different structures and molecules, different sets must be selected accordingly to control macroscopic conditions such as temperature and pressure.

The dynamic simulation in this paper mainly adopts the Berenson constant temperature variable method and proportional coefficient constant pressure method to control.

(1) Berenson variable scale thermal bath method. This method performs temperature control by connecting the analog system to a thermostatic bath with a temperature of

T. This means that the heat exchange rate is proportional to the temperature difference between the two.

$$\frac{dT(t)}{dt} = \frac{T_0 - T(t)}{\tau}. \quad (2)$$

1 is called the relaxation time, and the smaller the equilibrium time, the shorter (usually choose c~0. lps). As mentioned earlier, the dynamic simulation uses the difference formula to approach the differential equation step by step. Here, Taylor's expansion and Fourier's law are used to expand in 2 places to solve the problem:

$$T(t) = T_0 + (T(0) - T_0)e^{-t/\tau}, \quad (3)$$

$$\frac{T(t + \Delta t/2)}{T(t - \Delta t/2)} = \lambda^2, \quad (4)$$

where 3 is the acceleration factor.

2.5. Principles of Simulation Calculation. The basic principle of molecular dynamics is to first reflect all kinds of particles to its original position and momentum and then adjust the motion rules of these particles to completely obey the Newtonian equation of motion [28]. The data can be used to solve the equations to obtain displacement, velocity, and acceleration. The principles of statistical physics calculate system mechanics, thermodynamics, kinetics, and their properties.

Imagine a system composed of N particles; the sum of the total kinetic energy and kinetic energy of the particles is the total kinetic energy of the entire system. According to Newton's second law, the acceleration of particle i is

$$a = \frac{F}{m}. \quad (5)$$

According to classical mechanics, force 1 received by each particle i is the negative gradient of the potential energy function U:

$$F_i = -\nabla_i U. \quad (6)$$

It can be seen from the above that the basic principle of molecular dynamic modeling is to first obtain the dynamic ability of the particles from the relative position of the moving particles and then calculate the force acting on the particles and the acceleration of motion by Newton's second law. After that, through the original velocity and initial displacement, the velocity and displacement after time t can be obtained, and then, through repeated cycles, the velocity and displacement of new particles can be obtained every day. The basic principle of solving the Newtonian equation of motion above is to resolve a normal quadratic differential equation step by step through the finite difference method in a very short time step. Some classic calculations are summarized below.

(1) The Verlet algorithm is usually the simplest and is loved by many researchers. Its generation is the result of Taylor's expansion of particle coordinates at time t:

$$r(t + \Delta t) = r(t) + V(t)\Delta t + \frac{1}{2!}a(t)(\Delta t)^2 + \cdots, \quad (7)$$

$$r(t + \Delta t) = r(t) - V(t)\Delta t + \frac{1}{2!}a(t)(\Delta t)^2 + \cdots \quad (8)$$

Add the two equations together to get

$$r(t - \Delta t) = -r(t - \Delta t) + 2r(t) + a(t)(\Delta t)^2 \quad (9)$$

3. Mathematical Model and Simulation Calculation Method Based on the Exfoliation of Single-Layer Graphene from Dispersed Carbon Nanotubes

3.1. The Idea of Exfoliating Single-Layer Graphene with Dispersed Carbon Nanotubes

(1) Establish a mathematical model based on the high-speed centrifugal motion of the crushing sphere in the crushing cavity and the motion trajectories of the collision sphere and the shear sphere

(2) The centrifugal shear strength is calculated according to the model

(3) Calculate the scattering limit length of the blind zone between the spheres based on the model, that is, the boundary scattering zone

3.2. Preparation Process. Take 0.8 kg of carbon nanotube powder, 3 kg of dispersant, and 20 m of solvent, and the solvent is NMP. After the above materials are stirred and dispersed in the dispersion tank, they are continuously transported to the 30-liter crusher through a constant-speed diaphragm pump and a 30-liter crusher. The inner cavity is straight 244 mm. In the crusher, the material is continuously supplied to the crusher in a continuous crushing mode. The crusher continuously crushes and outputs the crushed materials at the same time and be crushed and dispersed at a high speed of 11 m/s for 10 hours to form a viscous dispersion of carbon nanotubes.

3.3. Establishment of Carbon Nanotube Model. The carbon tube has a hexagonal crystal structure. Each carbon atom in the carbon nanotube is connected by three other connected carbon atoms, among which the sp two-hybridization is the most important. Single-walled carbon nanotubes can also produce graphene-level mapping, so that the regular hexagonal lattice of carbon nanotubes forms a certain angle with the axis. In other words, the carbon nanotubes now appear to be spiral and have chiral characteristics.

It can be divided into three types: sawfish type, armchair type, and spiral type.

In this article, the Materials Studio modeling software is used to create carbon nanotube models and hybrid carbon nanotubes with different structural parameters. The diameter of the carbon nanotube structure is 8.14 A and the length is 120.52 A.

3.4. Centrifugal Friction Shear Strength. The simulation calculation method provided in this article is based on the rapid centrifugal movement of the crushing balls in the crushing chamber. The balls collide with each other and shear, peel off the single-wall graphene, and disperse the carbon nanotubes. The mathematical model of collision and friction between spheres calculates the shear strength 1 between spheres as follows.

$$P_d = \frac{F_c}{(1/2)S_q} = \frac{4\rho v^2 r^2}{3R^2}, \tag{10}$$

$$n_i = \frac{V_1}{V_2} = \frac{3m}{4\rho\pi r^3}, \tag{11}$$

$$\sum P = n_i P_d = \frac{mv^2}{\pi R^2 r}, \tag{12}$$

where 1 is the linear velocity of the centrifugal movement of the sphere, R is the radius of the grinding cavity, r is the radius of the sphere, 2 is the shear friction between the two spheres, and S sphere is the surface sphere of the grinding cavity. V is the volume of a single sphere, 5 is the density of the sphere, 3 is the shear strength of the friction between the spheres, 6 is the number of spheres, m is the total mass of the sphere, and 4 is the shear force and the shear strength between the total friction.

3.5. The Dispersion Limit Length of the Dispersion Limit Zone. Table 1 takes a 30 L grinder with a direct inner cavity of 244 mm and a linear velocity of 11 m/s as an example to calculate the selection of balls and the limit dispersion table:

From the data in Table 1, we can see that when the diameter of the sphere is less than 1.2μm, the dispersion limit length of the limit dispersion zone is less than 1μm. In other words, the dispersion is performed at the nanometer level. The diameter r of the sphere is less than 0.38μm, and the shear strength reaches the limit value of 650.12 GPa, which is the peeling of graphite flakes. The toner flakes are peeled to form a single layer of graphene dispersed in the liquid.

3.6. Stripping Parameters. The grinding process contains a variety of process parameters that need to be balanced and controlled, such as graphene exfoliation and carbon nanotube diffusion. Through the peeling and diffusion effects after the test, the main parameters of the entire processing flow are determined. After the process parameters are selected, the process parameters need to be strictly controlled to achieve graphene exfoliation and carbon nanotube diffusion. Due to the change of process parameters, the results of delamination and diffusion will be quite different.

3.7. Graphene Detection Method

(1) At present, graphene characterization mainly includes graphene morphology characterization and thickness characterization. The UV spectrophotometer mainly measures the absorbance and concentration of the graphene dispersion obtained by the liquid phase separation method. XRD is used as a tool for measuring crystallinity and interplanar spacing. The 2θ angle of the crystal can be combined with the Bragg equation to calculate the interplanar spacing of the crystal, and the change in the crystal structure can be inferred from the change in 2θ. Graphite is a stable structure formed by stacking graphene sheets, $2\theta = 26.6^\circ$, and the corresponding interplanar spacing is 0.335 nm. When graphite is exfoliated into graphene, the structure of graphite is destroyed, and the peak intensity of graphite at 26.6° is significantly reduced, the peak shape becomes wider, and the intensity and peak can be reduced. The Raman spectrum of graphene contains different D and G peaks. The degree of graphene defects can be judged by the ratio of the D peak to the G peak. The greater the ratio of the two, the greater the defect. XPS can measure the carbon and oxygen content of graphene. Generally speaking, the higher the oxygen content of graphene, the higher the degree of substitution of the original structure of graphene, and the larger the defects in graphene. The Raman and XPS characterization results are complementary to each other. Both SEM and HR-TEM can characterize the external shape of graphene nanosheets. Among them, SEM can measure the internal shape and area of graphene nanosheets and characterize the external shape of multiple graphene sheets, but because of the low resolution, the detailed internal structure of each graphene sheet cannot be clearly seen. HR-TEM's ultrahigh resolution technology can overcome this problem. In the HR-TEM graph, the shape and thickness of the graphene sheet can be clearly seen, and the number of internal grid patterns can be known by magnifying the edge of the graphene sheet and determining the number of graphene layers. At the same time, HR-TEM's selected area electron diffraction (SAED) technology can also make people distinguish single-layer, double-sided, and multilayer graphene. AFM can measure the internal thickness of graphene nanosheets. This function also makes it a powerful tool to characterize the number of graphene layers. By combining the thickness of single-layer graphene, the number of multilayer graphene sheets can be measured, and the distribution of the thickness and number of layers of the prepared graphene nanosheets can be calculated through mathematical statistics of specific numbers

Table 1: Select ball and limit dispersion table.

Ball diameter (μm)	Friction shear strength (GPa)	Dispersion limit length l (um)	Remark
1.41	184.98	1.10	Micron dispersion
1.22	215.73	0.95	
1.12	258.98	0.79	Nanodispersion (dispersion of carbon nanotubes)
0.61	431.55	0.49	
0.42	647.23	0.32	Nanodispersion, there will be flattening and tearing phenomenon (exfoliation of single-layer graphene)
0.39	650.12	0.31	

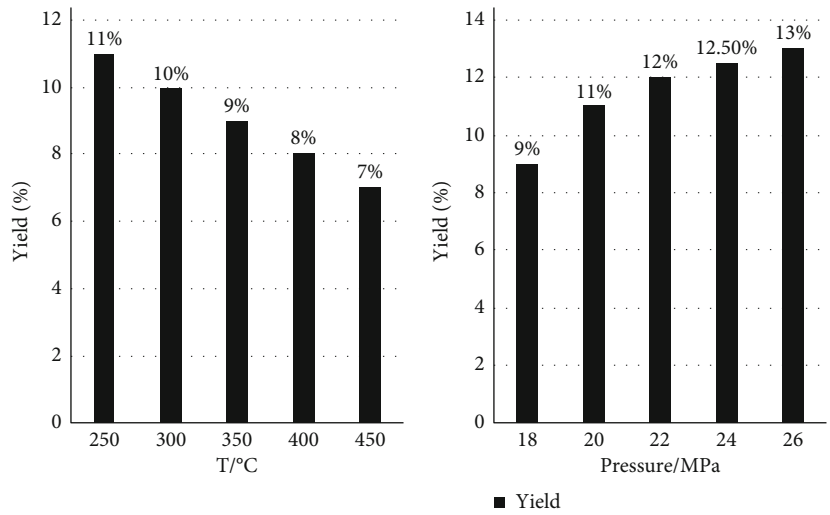

Figure 4: Influence of preparation conditions on the effect of exfoliating single-layer graphene.

Table 2: Effect of speed on graphene production during centrifugation.

Entry	Rotating speed (rpm)	Time (min)	Yield (%)
1	500		15
2	1000	35	11
3	1500		7

(2) UV-Vis is one of the most commonly used methods to characterize the concentration of graphene. According to Lambert's law, the absorbance of a dilute solution is directly proportional to the thickness of the liquid layer and the concentration of the substance. The reason for being limited to dilute solutions is that the average distance between substances increases at high concentrations, and individual graphene particles are affected by neighboring particles and their charges, changing their ability to absorb specific radiation

4. Based on the Effect of Stripping Single-Layer Graphene from Dispersed Carbon Nanotubes

4.1. The Influence of Preparation Conditions on the Effect of Exfoliating Single-Layer Graphene

(1) The influence of various temperature and pressure variables on the performance of graphene is studied, and the experimental results are shown in Figure 4

As shown in Figure 4, at a high temperature of 250°C, the rate of graphene formation is about ten percent. When the high temperature rises to 450°C, the rate of graphene formation is reduced from 10% to 7%. When the high temperature exceeds 450°C, the solvent decomposes in a large amount. But facts have also proved that high temperature is not conducive to graphene peeling. Due to the increase in pressure, the utilization rate of graphene has increased. When the pressure rises by 26 MPa (the maximum operating pressure allowed by the reactor), the utilization rate of graphene will reach 12%. High pressure may also be thought to help exfoliate graphene.

(2) A brief study of the influence of speed on graphene output during centrifugation is shown in Table 2

It can be seen from Table 2 that under the same reaction conditions and the same separation time, the yield of graphene samples is 15% when the speed is 500 rpm, the yield of graphene samples is 11% when the speed is 1000 rpm, and the yield of graphene samples is 1500 rpm when the speed is 1500 rpm. The rate is 7%. The yield of graphene samples decreases as the rotation speed increases.

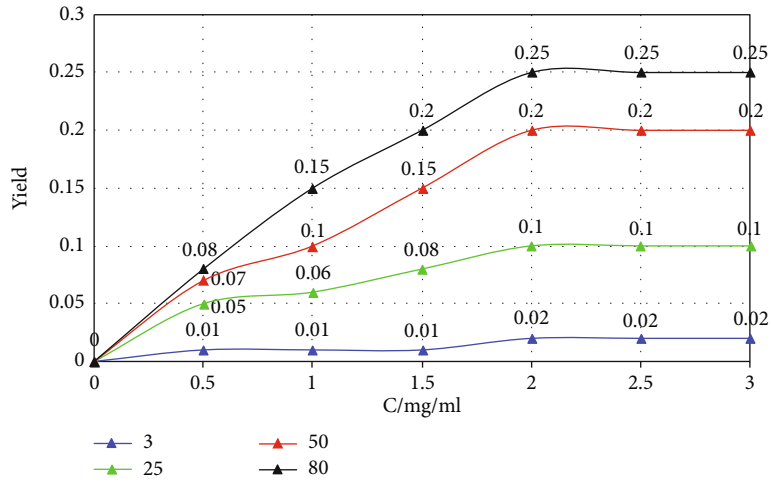

Figure 5: Influence of the amount of dispersing aids on the effect of exfoliating single-layer graphene.

Table 3: Calculated value of excess molar volume.

Water volume fraction (Vw)	Density	Excess molar volume
1.0	0.997	0.00
0.9	0.999	-0.10
0.8	1.002	-0.25
0.7	1.005	-0.44
0.6	1.008	-0.67
0.5	1.010	-0.96
0.4	1.011	-1.22
0.3	1.001	-1.61
0.2	0.998	-154
0.1	0.982	-1.23

4.2. The Influence of the Amount of Dispersing Aids on the Peeling Effect of Single-Layer Graphene. The system was prepared with different concentrations of dispersing aids and peeled at 3500 rpm for 15 minutes and then centrifuged at 1100 rpm for 35 minutes to obtain a graphene dispersion. The law of concentration is shown in Figure 5.

It can be seen from Figure 5 that, as the concentration of the dispersant increases, the concentration begins to decrease and eventually stabilizes and no longer changes. The initial increase in the concentration of the dispersion aid is due to the fact that it provides more stabilizers for the adsorption of the graphene surface, resulting in an increase in the stability of the dispersed graphene. However, when the polymer concentration exceeds the critical value (2 mg/mL), the dispersed graphene concentration does not increase but decreases. This phenomenon is because the excess dispersant molecules entangle with each other to form supramolecular structures such as micelles. The supramolecules are too large to enter the outer layer of the space graphene sheet, and as a result, the amount of graphene dispersed does not increase. In short, the optimal dispersion concentration of 2 mg/mL is selected and then determined as a constant process parameter.

4.3. Stability of Graphene Dispersion. Under normal circumstances, the stability of solute molecules (hereinafter referred to as graphene) in solution mainly depends on three kinds of interactions: the interaction between the solvent and the solute, the interaction between the solvent and the solvent, and the interaction between the solute. In the mixed solvent system, the solvent-cosolvent interaction also has a significant impact on the solvent-solute interaction and solute stability. Excess molar volume, as a kind of excess thermodynamic force, and excess molecular volume may reflect the interaction between molecules in the mixture. For a mixed system of water and TMU, the excess molecular weight can be calculated by the following formula. Table 3 shows the calculated value of excess molar volume.

$$V^E = [xM_1 + (1-x)M_2]\rho - xM_1\rho_1 - (1-x)M_2\rho_2. \quad (13)$$

In the formula, 1 and 2 represent the density of water, TMU and water-TMU and mixed solvent, respectively, and 3 and 4 represent the density of water and TMU, respectively.

It can be seen from Table 3 that when the volume fraction of water is 0.3, the excess molecular volume of the mixed solvent is the minimum, and the dispersion concentration of graphene is the maximum.

The concentration of the dispersion aid is selected as 2 mg/mL, and the relationship between the eccentricity of the graphene concentration (left) and the sedimentation time (right) is obtained. The initial graphite concentration is 80 mg/mL, the shear removal time is 15 minutes, and the solution is left for 6 hours. Remove the supernatant and centrifuge at different speeds for 35 minutes. Take the supernatant and measure the absorbance. After calculating the concentration, take the supernatant and observe the concentration of the graphene dispersion after different precipitation times. The results are shown in Figure 6.

It can be seen from Figure 6 that the graphene concentration is inversely proportional to the eccentricity. If the centrifugation speed is slow, a high-concentration graphene

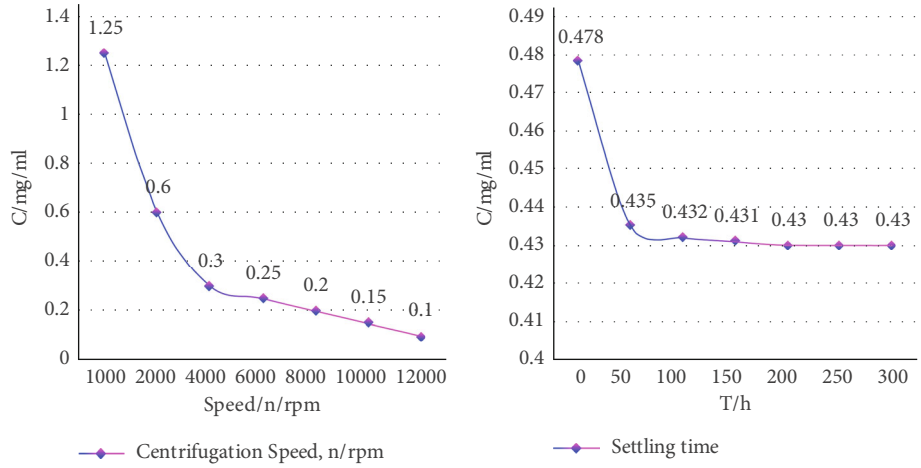

Figure 6: Stability of graphene dispersion.

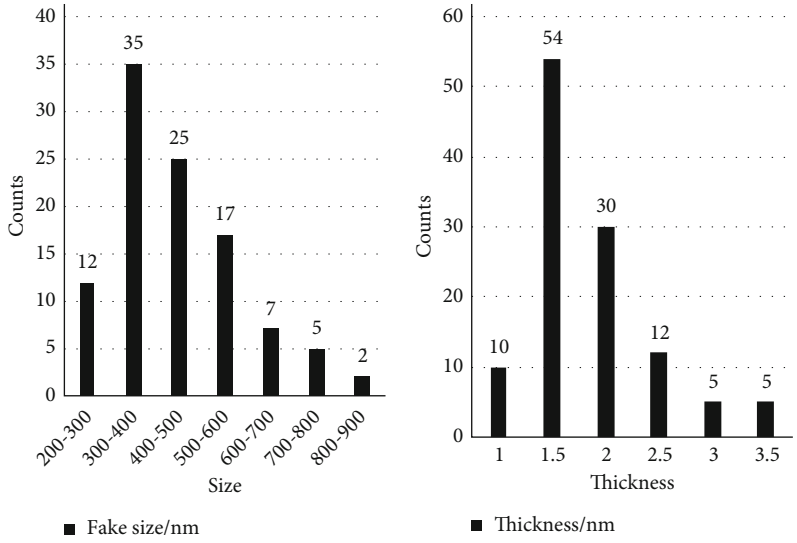

Figure 7: Evaluation results of graphene peeling state.

dispersion can be obtained. On the contrary, the obtained graphene concentration is low. In the actual preparation process, the concentration and stability of the graphene dispersion are the most significant factors. At high eccentricity, the graphene dispersion is very stable, but the concentration is low. The obtained graphene has a high concentration, but the dispersibility is unstable. Precipitation experiments show that after 2 days at room temperature, about 96% of graphene is still stably dispersed in the system. This indicates that the entire system is in a stable state.

4.4. Evaluation of the Exfoliation State of Graphene. The AFM and TEM testing methods were used to characterize the exfoliation state of graphene, and the resulting sheet size distribution and thickness distribution are shown in Figure 7.

It can be seen from Figure 7 that more than half of the graphene sheets are 300-500 nanometers in size, and more than 80% of the graphene sheets are about 1.5 nanometers in size. The thickness of a single layer of pure graphene is 0.6-0.9 nm, and the thickness of each layer is slightly larger than that of pure graphene, because the graphene sheet here adsorbs a dispersion aid. Thickness statistics show that most of the graphene obtained in the experiment is single-layer, double-layer, and a very small part of graphene with few layers.

5. Conclusions

This article focuses on the exfoliation of single-layer graphene based on dispersed carbon nanotubes. This paper establishes a mathematical model based on the high-speed centrifugal motion of the crushing ball in the crushing cavity and the motion trajectories of the collision ball and the shearing ball. According to the model, the centrifugal shear strength and the scattering limit length of the blind zone between the spheres are calculated, that is, the boundary scattering region. After understanding the relevant theories,

the exfoliated single-layer graphene based on dispersed carbon nanotubes is analyzed, and then, the exfoliated single-layer graphene based on this method is examined. The test results show that the thickness of each layer of the graphene stripped in this paper is slightly larger than that of pure graphene, because the graphene sheet here adsorbs the dispersion aid, and most of the graphene stripped in the experiment is in a single-layer and double-layer layers; very few of them are multilayered. Most of the data in this study are from data sources, but a small part of the data does not have sufficient evidence to prove that it is true and effective.

Data Availability

No data were used to support this study.

Conflicts of Interest

The authors declare that there are no conflicts of interest regarding the publication of this article.

References

[1] D. Voiry, J. Yang, J. Kupferberg et al., "High-quality graphene via microwave reduction of solution-exfoliated graphene oxide," *Science*, vol. 353, no. 6306, pp. 1413–1416, 2016.

[2] Z. M. Markovic, "Semi-transparent, conductive thin films of electrochemical exfoliated graphene," *RSC Advances*, vol. 6, no. 45, pp. 39275–39283, 2016.

[3] M. P. Weir, D. W. Johnson, S. C. Boothroyd et al., "Extrinsic wrinkling and single exfoliated sheets of graphene oxide in polymer composites," *Chemistry of Materials*, vol. 28, no. 6, pp. 1698–1704, 2016.

[4] T. Tomašević-Ilić, J. Pešić, I. Milošević et al., "Transparent and conductive films from liquid phase exfoliated graphene," *Optical and Quantum Electronics*, vol. 48, no. 6, 2016.

[5] Z. S. Metaxa, "Exfoliated graphene nanoplatelet cement-based nanocomposites as piezoresistive sensors: influence of nanoreinforcement lateral size on monitoring capability," *Ciência & Tecnologia dos Materiais*, vol. 28, no. 1, pp. 73–79, 2016.

[6] T. Zhan, X. Wang, X. Li, Y. Song, and W. Hou, "Hemoglobin immobilized in exfoliated Co_2Al LDH-graphene nanocomposite film: Direct electrochemistry and electrocatalysis toward trichloroacetic acid," *Sensors and Actuators B Chemical*, vol. 228, pp. 101–108, 2016.

[7] X. Xu, B. Karami, and D. Shahsavari, "Time-dependent behavior of porous curved nanobeam," *International Journal of Engineering Science*, vol. 160, article 103455, 2021.

[8] T. Kavinkumar and S. Manivannan, "Uniform decoration of silver nanoparticle on exfoliated graphene oxide sheets and its ammonia gas detection," *Ceramics International*, vol. 42, no. 1, pp. 1769–1776, 2016.

[9] A. Radocea, T. Sun, T. H. Vo, A. Sinitskii, N. R. Aluru, and J. W. Lyding, "Solution-synthesized chevron graphene nanoribbons exfoliated onto H:Si(100)," *Nano Letters*, vol. 17, no. 1, pp. 170–178, 2017.

[10] Y. Ma, D. Bai, X. Hu et al., "Robust and antibacterial polymer/mechanically exfoliated graphene nanocomposite fibers for biomedical applications," *ACS Applied Materials & Interfaces*, vol. 10, no. 3, pp. 3002–3010, 2018.

[11] A. Sham and S. M. Notley, "Adsorption of organic dyes from aqueous solutions using surfactant exfoliated graphene," *Journal of Environmental Chemical Engineering*, vol. 6, no. 1, pp. 495–504, 2018.

[12] C. I. Idumah, A. Hassan, and S. Bourbigot, "Influence of exfoliated graphene nanoplatelets on flame retardancy of kenaf flour polypropylene hybrid nanocomposites," *Journal of Analytical and Applied Pyrolysis*, vol. 123, pp. 65–72, 2017.

[13] G. T. Usca, J. Hernandez-Ambato, C. Pace, L. S. Caputi, and A. Tavolaro, "Liquid-phase exfoliated graphene self-assembled films: low-frequency noise and thermal-electric characterization," *Applied Surface Science*, vol. 380, pp. 268–273, 2016.

[14] L. Zeng, J. Shi, J. Luo, and H. Chen, "Silver sulfide anchored on reduced graphene oxide as a high-performance catalyst for CO_2 electroreduction," *Journal of Power Sources*, vol. 398, pp. 83–90, 2018.

[15] Z. Ji, M. Perez-Page, J. Chen, and S. Holmes, "Nitrogen doped reduced electrochemically exfoliated graphene oxide inserted carbon black as novel catalyst support for the hydrogen fuel cell," *ECS Meeting Abstracts*, vol. MA2020-02, no. 36, pp. 2323–2323, 2020.

[16] S. Mypati, A. Sellathurai, M. Kontopoulou, A. Docoslis, and D. P. J. Barz, "Synthesis and performance evaluation of exfoliated graphene nanoplatelet hydrogels as electrodes for supercapacitors," *ECS Meeting Abstracts*, vol. MA2020-01, no. 10, pp. 863–863, 2020.

[17] Á. Gallardo-López, J. Castillo-Seoane, C. Muñoz-Ferreiro, C. López-Pernía, A. Morales-Rodríguez, and R. Poyato, "Flexure strength and fracture propagation in zirconia ceramic composites with exfoliated graphene nanoplatelets," *Ceramics*, vol. 3, no. 1, pp. 78–91, 2020.

[18] M. D. Nurhafizah, A. A. Aziz, A. B. Suriani, A. Mohamed, and T. Soga, "Low-temperature exfoliated graphene oxide incorporated with different types of natural rubber latex: electrical and morphological properties and its capacitance performance," *Ceramics International*, vol. 46, no. 5, pp. 5610–5622, 2020.

[19] P. Wang, T. Yao, Z. Li et al., "A superhydrophobic/electrothermal synergistically anti-icing strategy based on graphene composite," *Composites Science and Technology*, vol. 198, article 108307, 2020.

[20] J. You, B. Oh, Y. S. Yun, and H.-J. Jin, "Improvement in barrier properties using a large lateral size of exfoliated graphene oxide," *Macromolecular Research*, vol. 28, no. 8, pp. 709–713, 2020.

[21] A. Islam, B. Mukherjee, K. K. Pandey, and A. K. Keshri, "Ultrafast, chemical-free, mass production of high quality exfoliated graphene," *ACS Nano*, vol. 15, no. 1, pp. 1775–1784, 2021.

[22] Q. Cui, P. Thakur, C. Rablau, I. Avrutsky, and M. M. C. Cheng, "Miniature optical fiber pressure sensor with exfoliated graphene diaphragm," *IEEE Sensors Journal*, vol. 19, no. 14, pp. 5621–5631, 2019.

[23] A. Kaur and R. C. Singh, "Temperature sensor based on exfoliated graphene sheets produced by microwave assisted freezing induced volumetric expansion of carbonated water," *Journal of Materials Science: Materials in Electronics*, vol. 30, no. 6, pp. 5791–5807, 2019.

[24] J. Gnidakouong, X. Gao, A. Kafy, J. Kim, and J. H. Kim, "Fabrication and electrical properties of regenerated cellulose-loaded exfoliated graphene nanoplatelet composites," *Carbon Letters*, vol. 29, no. 2, pp. 115–122, 2019.

[25] M. Ahmed and T. Imae, "Effect of external magnetic field on cyclic voltammetry of exfoliated graphene-based magnetic composites with conductive polymer and carbon dots," *Journal of Magnetism and Magnetic Materials*, vol. 491, article 165604, 2019.

[26] V. Vasanthi, T. Logu, V. Ramakrishnan, K. Anitha, and K. Sethuraman, "Study of electrical conductivity and photoelectric response of liquid phase exfoliated graphene thin film prepared via spray pyrolysis route," *Carbon Letters*, vol. 30, no. 4, pp. 1–7, 2019.

[27] X. Xu and Y.-L. Hsieh, "Aqueous exfoliated graphene by amphiphilic nanocellulose and its application in moisture-responsive foldable actuators," *Nanoscale*, vol. 11, no. 24, pp. 11719–11729, 2019.

[28] C. Deng, X. Wang, Y. Shan, and Z. Song, "Study on the effect of low molecular hydrocarbon compounds on coal spontaneous combustion," *Fuel*, vol. 318, article 123193, 2022.